

Nonlinear resonances phenomena in a modified Josephson junction model

Pernel Nguenang, Sandrine Takam Mabekou, Patrick Louodop, Arthur Tsamouo Tsokeng, and Martin Tchoffo
Citation: Chin. Phys. B, 2020, 29 (**12**): 120501. DOI: 10.1088/1674-1056/aba9cd
Journal homepage: http://cpb.iphy.ac.cn; http://iopscience.iop.org/cpb

What follows is a list of articles you may be interested in

Chaotic signal denoising algorithm based on sparse decomposition

Jin-Wang Huang(黄锦旺), Shan-Xiang Lv(吕善翔), Zu-Sheng Zhang(张足生), Hua-Qiang Yuan(袁华强)
Chin. Phys. B, 2020, 29 (**6**): 060505. DOI: 10.1088/1674-1056/ab8a3b

Hidden attractors in a new fractional-order discrete system: Chaos, complexity, entropy, and control

Adel Ouannas, Amina Aicha Khennaoui, Shaher Momani, Viet-Thanh Pham, Reyad El-Khazali
Chin. Phys. B, 2020, 29 (**5**): 050504. DOI: 10.1088/1674-1056/ab820d

Novel Woods-Saxon stochastic resonance system for weak signal detection

Yong-Hui Zhou(周永辉), Xue-Mei Xu(许雪梅), Lin-Zi Yin(尹林子), Yi-Peng Ding(丁一鹏), Jia-Feng Ding(丁家峰), Ke-Hui Sun(孙克辉)
Chin. Phys. B, 2020, 29 (**4**): 040503. DOI: 10.1088/1674-1056/ab75ca

Nonlinear continuous bi-inductance electrical line with dissipative elements: Dynamics of the low frequency modulated waves

S M Ngounou, F B Pelap
Chin. Phys. B, 2020, 29 (**4**): 040502. DOI: 10.1088/1674-1056/ab75d6

Dynamical response of a neuron-astrocyte coupling system under electromagnetic induction and external stimulation

Zhi-Xuan Yuan(袁治轩), Pei-Hua Feng(冯沛华), Meng-Meng Du(独盟盟), Ying Wu(吴莹)
Chin. Phys. B, 2020, 29 (**3**): 030504. DOI: 10.1088/1674-1056/ab7441

Nonlinear resonances phenomena in a modified Josephson junction model

Pernel Nguenang[1], Sandrine Takam Mabekou[2], Patrick Louodop[1,3], Arthur Tsamouo Tsokeng[1], and Martin Tchoffo[1,†]

[1] *Research Unit Condensed Matter, Electronics and Signal Processing, The University of Dschang, P. O. Box 67 Dschang, Cameroon*
[2] *Unité de Recherche de Mécanique et de Modélisation des Systèmes Physiques (UR-2MSP), Faculté des Sciences, Université de Dschang, BP 69 Dschang, Cameroun*
[3] *São Paulo State University (UNESP), Instituto de Física Teórica, Rua Dr. Bento, Teobaldo Ferraz 271, Bloco II, Barra Funda, 01140 – 070 São Paulo, Brazil*

(Received 4 May 2020; revised manuscript received 11 July 2020; accepted manuscript online 28 July 2020)

In this paper, the equivalent circuit of the non-autonomous Josephson junction (JJ) is presented and the effect of the proper frequency on the phase ϕ is studied. We also study nonlinear resonance phenomena in the oscillations of a modified Josephson junction (MJJ). These oscillations are probed through a system of nonlinear differential equations and the multiple time scale method is employed to investigate all different types of resonance that occur. The results of primary, superharmonic and subharmonic resonances are obtained analytically. We show that the system exhibits hardening and softening behaviors, as well as hysteresis and amplitude hopping phenomena in primary and superharmonic resonances, and only the hysteresis phenomenon in subharmonic resonance. In addition, the stabilities and the steady state solutions in each type of resonances are kindly evaluated. The number of equilibrium points that evolve with time and their stabilities are also studied. Finally, the equations of motion are numerically integrated to check the correctness of analytical calculations. We further show that the dynamics of the MJJ is strongly influenced by its parameters.

Keywords: nonlinear resonances, hysteresis and jump phenomena, modified Josephson junction

PACS: 05.45.–a, 03.75.Lm **DOI:** 10.1088/1674-1056/aba9cd

1. Introduction

Nonlinear oscillations have been studied analytically and numerically with applications in the fields of physics, chemistry, and engineering.[1–3] Studying their dynamics is often very difficult even though they are exciting. One of the major problem in this theory of nonlinear oscillations lies in the search for possibilities to estimate both amplitude and time analytically.[4] Hence, several nonlinear oscillators have significantly attracted the attention of researchers, such as the Rayleigh–Duffing oscillator and the Van-der Pol oscillator, just to list a few.[1,5–7] The interest in studying the dynamical behavior (for example, the response of harmonic, subharmonic, and superharmonic resonances) of such systems comes from the appearance of strong nonlinearity in the differential equations governing their dynamics.[6,8,9] However, particular interests are given to some important phenomena that most often occur in those systems when studying their dynamics. Here we refer to hysteresis, amplitude jump, resonance, multi-resonance, and stability phenomena that are regularly observed.[10–12]

Besides the Rayleigh–Duffing and Van-der Pol oscillators where the above mentioned phenomena have already been studied, there is also the well known Josephson junction (JJ), which is a nonlinear oscillator with some special properties from its dynamics.[13] Josephson effects are phenomena that appear when two superconductors are separated by a thin layer of non-superconducting materials.[14,15] Nevertheless, this particular phenomenon has been deeply studied in the literature, and it comes that the equivalent diagram of the ordinary JJ is a circuit made of three components (R_j, C_0, and $\sin(\phi)$), which are connected in parallel each to other.[16–18] However, several questions are the subject of ongoing research to make their implementation easy. That is, it is important to study the amplitudes of oscillation and the harmonic content of Josephson sources to produce oscillators with high power and narrow line widths. Also, situations in which several Josephson oscillators can be locked in phase to provide higher output power is still a big challenge to researchers. As such, superconducting JJ arrays present an advantage as model systems for studying coupling between nonlinear oscillators as well as possible sources of high frequency oscillator.[19] Moreover, other applications of JJ include submillimeter and millimeter wave oscillators.[20] Ordinary JJ, although may not have a natural frequency, can present harmonic oscillations.[20–23] To compensate this, Louodop *et al.*[24] proposed a modified Josephson junction (MJJ) model.

This circuit has an interesting feature which is the presence of five electrically speaking state variables $\dot{\phi}$ (the voltage across the capacitors), three capacitors C_1, C_2, and C_j and the current flowing through the coil $i(t)$. However, the dynamics of the entire oscillator resumes to two state variables, which are ϕ and V_j. Taking into account the mathematical expres-

†Corresponding author. E-mail: mtchoffo2000@yahoo.fr

© 2020 Chinese Physical Society and IOP Publishing Ltd

sions obtained in Ref. [24], there is a very strong resemblance to the ordinary JJ model as described in Refs. [16–18], with two new terms including a_3 which plays the role of the proper frequency in the usual model and p is a constant. In Ref. [24], it was shown that such circuit exhibits an extreme multistability behavior. Our objective is therefore to show the influence of the newly added parameter a_3 on our model which constitute the modified form of the ordinary JJ.

Thus, based on this MJJ model, we propose in this paper an equivalent circuit, which presents two new elements, namely a current source with controlled phase $\phi(t)/L$ and a source of direct current pC. In addition, we study the nonlinear dynamical behavior that may exhibit the system with the help of the multiple time scale method.[10]

To achieve this objective, we therefore organised the paper as follows: In Section 2, we present the circuit and model of the MJJ. Section 3 presents the equivalent model of the MJJ. In Section 4, we mathematically analyze different types of resonance occurring in this circuit. In Section 5, we study the effects of each parameter of the system on each type of resonance. Finally, Section 6 concludes the work.

2. Circuit and the equivalent model of the modified Josephson junction

The electrical device used here is an MJJ recently published in Ref. [24]. Its dimensionless system of differential equations is given as follows:

$$\begin{aligned}\dot{x}_1(\tau) &= x_2(\tau),\\ \dot{x}_2(\tau) &= \beta(e_0\omega\sin(\omega\tau) - a_1\sin(x_1(\tau))\\ &\quad - a_2x_2(\tau) - a_3x_1(\tau)) - \beta p,\end{aligned} \tag{1}$$

where e_0 is the amplitude of $\dot{e}(t)/2$, $t = \Omega\tau$, $\beta = 2\Omega C/(C+2C_j)$ with Ω a well chosen constant, $a_1 = 1/C$, $a_2 = 1/R_jC$, $a_3 = 1/LC$, and $p = (1/LC)\phi(0) - (1/C)i(0)$.

Recently, You and Nori[25] modelled the JJ as an internal inductor, which means that L_j is connected in parallel with the phase controlled current source $\sin(\phi)$. A similar idea was previously developed by Kaplunenko and Fischer[26] in 2004. Since our circuit has an external inductor L in parallel with the JJ (see Fig. 1), it can be considered that the overall system is made of two inductors in parallel: an implicit one L_j, and an explicit one L, with the resulting inductor value of $L_{\rm eq} = L_jL/(L_j+L)$. For the circuit in Fig. 1, the equivalent inductor is closer or almost equal to the internal inductor L_j, which is of the order of pico-Henry (pH) according to Ref. [26]. If L is large enough, the current given by Eq. (7) of Ref. [24] becomes sufficiently small. From this equation, we realize that $i(t)$ linearly depends on $\phi(t)$ and therefore, this current could be used to study the dynamics of the phase, acting as a phasemeter of the JJ.

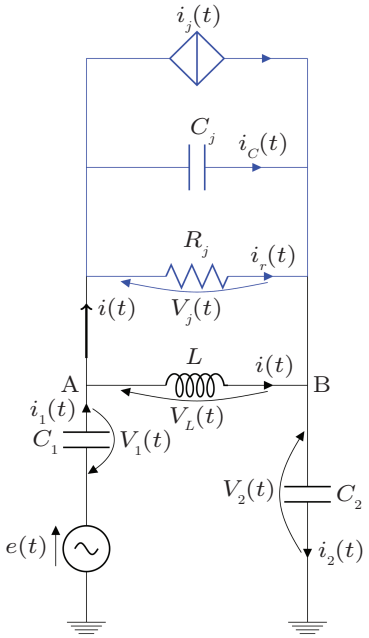


Fig. 1. Schematic diagram of the modified JJ extreme multistable circuit.[24]

Figure 2(a) shows the time dependence of the phase of the MJJ depicted in Fig. 1. For the parameters $a_3 = 2\times10^{-6}$ and $p = 10^{-5}$, (see Fig. 2(a)) the signal $x_1(\tau)$ presents a very low frequency and a high amplitude even if the dimensionless amplitude of the current flowing through the inductor L is around 0.01. Thus, $i(t)$ is negligible compared to $i_1(t)$ and $I(t)$. However, if L is sufficiently small, then the parameter βa_3 becomes the square of the natural frequency of the system, and we noticed by repeated simulations that the phase of the JJ becomes bounded, the frequency of the system increases, the amplitude of the phase becomes lower and the amplitude of $i(t)$ is non-negligible (see Fig. 2(b) where we set $a_3 = 0.2$ and $p = 10^{-3}$). The simulations were carried out with a time step of 0.005 and 10^7 iterations.

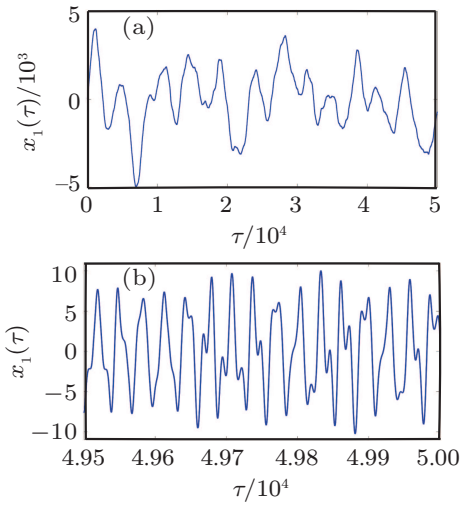


Fig. 2. Time histories of $x_1(\tau)$ for (a) $a_3 = 2\times10^{-6}$ and $p = 10^{-5}$ and (b) $a_3 = 0.2$ and $p = 10^{-3}$. The other parameters are $a_1 = 0.21$, $a_2 = 0.001$, $\beta = 1$, $w = 0.2$, and $e_0 = 1$ with the initial conditions $x_i(0) = 0$, $i = 1, 2$.

From the Kirchhoff laws on the electric device as shown

in Fig. 1, we get the following relations:

$$\dot{\phi}(t) = V_j(t), \tag{2a}$$

$$\frac{C+2C_j}{2}\dot{V}_j(t) = \frac{C\dot{e}(t)}{2} - \sin(\phi) - \frac{V_j(t)}{R_j} - \frac{1}{L}\phi(t) - pC. \tag{2b}$$

Considering $C_0 = (C+2C_j)/2$ and $I_0(t) = C\dot{e}(t)/2$, equations (2a) and (2b) take the following forms:

$$\dot{\phi}(t) = V_j(t), \tag{3a}$$

$$C_0\dot{V}_j(t) = I_0(t) - \sin(\phi) - \frac{1}{L}\phi(t) - \frac{V_j(t)}{R_j} - pC. \tag{3b}$$

A consequent interpretation of Eqs. (3a) and (3b) leads (by analogy to Ref. [25]) to the following AC equivalent circuit of the model shown in Fig. 3, which is an extended JJ. Here, with the external excitation source $I_0(t)$, the elements (R_j, C_0, and $\sin(\phi)$) are very close to those provided by JJ. The nonlinear term $\sin(\phi)$ is therefore an "internal" phase controlled current source. The remaining elements are assimilated to "external" phase controlled current source and a biasing direct current source $\phi(t)/L$ and pC respectively. Both "external" sources are induced by the presence of the inductor L in parallel with the JJ. The source pC is inductor L' initial conditions-dependent, which is a particular feature of the model.

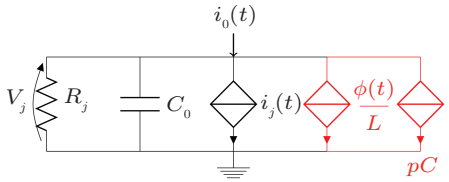


Fig. 3. Equivalent electrical circuit of the non-autonomous JJ-based Colpitt system. Compared with the JJ in Refs. [12–14], we have two new items (Red part of the circuit) a linear phase controlled current source $\phi(t)/L$ and a direct current source pC.

3. System analysis

Substituting the second equation of system (1) into the second derivative of the first one and performing a third-order expansion of the term $\sin(x_1(\tau))$, we obtain

$$\ddot{x}(\tau) + \omega_0^2 x(\tau) + \alpha x(\tau) - \frac{1}{6}\alpha x^3(\tau) + \mu\dot{x}(\tau) + \beta p = K\omega\sin(\omega\tau), \tag{4}$$

where $\alpha = \beta a_1$ is the nonlinearity parameter, $\mu = \beta a_2$ is the damping coefficient of the system, ω and $\omega_0^2 = \beta a_3$ are respectively the external and natural eigen-frequencies. $K = \beta e_0$ stands for the amplitude of the external excitation given to the system. The corresponding equation of motion governing the dynamics of the system is therefore given by

$$\ddot{x}(\tau) + \omega_0^2 x(\tau) = \varepsilon f(x,\dot{x}) + \omega E(\tau), \tag{5}$$

where ε is a small parameter,

$$f(x,\dot{x}) = \alpha x(\tau) + \frac{1}{6}\alpha x^3(\tau) - \mu\dot{x}(\tau) - \beta p$$

is a nonlinear function of x and $\dot{x}$ and $E(\tau) = K\sin(\omega\tau)$ is the so-called excitation force.

In general, when the external frequency is too close to the internal frequency, the phenomenon of resonance occurs. Therefore, the system oscillating with a large amplitude receives energy from external source. To approximate the solution of Eq. (5), we will use the method of multiple time scales (MMS). The analysis reveals the existence of various primary and secondary resonances (superharmonic and subharmonic).

3.1. Primary resonance state

In the case of primary resonance, we introduce a detuning parameter σ with a quantitative description of the proximity of ω to ω_0, instead of using the excitation frequency ω as a parameter. For this reason, we set $\omega = \omega_0 + \varepsilon\sigma$, and we assume a second order expansion of the solution with respect to ε as:

$$x(\tau,\varepsilon) = x_0(T_0,T_1) + \varepsilon x_1(T_0,T_1) + O(\varepsilon^2), \tag{6}$$

where $T_0 = \tau$, $T_n = \varepsilon^n T_0$, $n = 0,1,2,\ldots$. Then,

$$\frac{\mathrm{d}}{\mathrm{d}\tau} = D_0 + \varepsilon D_1 + O(\varepsilon^2),$$

$$\frac{\mathrm{d}^2}{\mathrm{d}\tau^2} = D_0^2 + 2\varepsilon D_0 D_1 + O(\varepsilon^2)$$

with $D_n^m = \partial^m/\partial T_n^m$. Substituting Eq. (6) into Eq. (5) and identifying the coefficients of the same powers, one obtains the following equations according to the orders $O(1)$ and $O(\varepsilon)$:

For $O(1)$ order, we have

$$D_0^2 x_0 + \omega_0^2 x_0 = 0. \tag{7}$$

And for $O(\varepsilon)$ order, we have

$$D_0^2 x_1 + \omega_0^2 x_1 = -2D_0 D_1 x_0 - \mu D_0 x_0 + \frac{1}{6}\alpha x_0^3 - \beta p - \alpha x_0 + K\omega_0\sin(\omega_0 T_0 + \sigma T_1). \tag{8}$$

The solution for Eq. (7) is given by

$$x_0 = A(T_1)\exp(\mathrm{i}\omega_0 T_0) + \bar{A}(T_1)\exp(-\mathrm{i}\omega_0 T_0), \tag{9}$$

where $A(T_1)$ is a complex-valued quantity that will be determined by imposing a resolution condition. By introducing the solution x_0 from Eq. (9) into Eq. (8) and expressing $\sin(\omega\tau)$ in the complex form, one obtains

$$D_0^2 x_1 + \omega_0^2 x_1 = \left[-\mathrm{i}\omega_0\left(2A' + \mu A\right) + \frac{1}{2}\alpha A^2 \bar{A} - \alpha A\right]\exp\left(\mathrm{i}\omega_0 T_0\right) + \frac{1}{6}\alpha A^3 \exp\left(3i\omega_0 T_0\right) - \beta p + \frac{1}{2\mathrm{i}} K \exp\left[\mathrm{i}\left(\omega_0 T_0 + \sigma T_1\right)\right] + \mathrm{CC}. \tag{10}$$

where A' indicates the derivative with respect to T_1 and CC is the complex conjugate of the previous terms. To eliminate secular terms from the particular solution of Eq. (10), we choose A to be a solution of the form

$$\mathrm{i}\omega_0\left(2A' + \mu A\right) - \frac{1}{2}\alpha A^2 \bar{A} + \alpha A - \frac{1}{2\mathrm{i}} K\omega_0 \exp\left(\mathrm{i}\sigma T_1\right) = 0. \tag{11}$$

In order to solve Eq. (11), let us choose A in the polar form as

$$A = \frac{1}{2} a \exp\left(\mathrm{i}\xi\right), \tag{12}$$

where ξ and a are real. The phase where $\gamma = \sigma T_1 - \xi$ and amplitude a of the response are governed by the following polar form of modulation equations

$$\begin{cases} a' = -\dfrac{1}{2}\mu a - \dfrac{K}{2}\cos\gamma, \\ \gamma' a = a\sigma + \dfrac{\alpha}{16\omega_0} a^3 - \dfrac{\alpha}{2\omega_0} a + \dfrac{K}{2}\sin\gamma, \end{cases} \tag{13}$$

where a' and γ' are the derivative with respect to the time scale T_1 of a and γ, respectively. To find the stable period solution, let $a' = \gamma' = 0$, then we obtain

$$\begin{cases} -\dfrac{1}{2}\mu a - \dfrac{K}{2}\cos\gamma = 0, \\ a\sigma + \dfrac{\alpha}{16\omega_0} a^3 - \dfrac{\alpha}{2\omega_0} a + \dfrac{K}{2}\sin\gamma = 0. \end{cases} \tag{14}$$

After some algebraic calculations, the frequency response in this primary state between a and σ can be rewritten as follows:

$$\left[\frac{1}{4}\mu^2 + \left(\sigma + \frac{\alpha}{16\omega_0} a^2 - \frac{\alpha}{2\omega_0}\right)^2\right] a^2 = \frac{K^2}{4}, \tag{15}$$

and the peak amplitude a_p of the primary response resonance obtained is given by

$$a_\mathrm{p} = \frac{K}{\mu}. \tag{16}$$

It is observed that the amplitude peak a_p is independent of the nonlinearity parameter α, and is also inversely proportional to μ. Increasing the value of μ consequently induces a decreasing of a_p.

For instance, let us study the stability of the motion of the steady-state by looking for the nature of the singular points of Eq. (13). For this purpose, let

$$\begin{aligned} a &= a_0 + a_1, \\ \gamma &= \gamma_0 + \gamma_1, \end{aligned} \tag{17}$$

where γ_0 and a_0 are respectively the values of γ and a in the steady state, γ_1 and a_1 are the slight variations of γ and a. Substituting Eq. (17) into Eq. (13) and developing for the small values of γ_1 and a_1, we get

$$\begin{aligned} a_1' &= -\frac{1}{2}\mu a_1 + \left(\frac{K}{2}\sin\gamma_0\right)\gamma_1, \\ \gamma_1' &= \left(\frac{\alpha}{8\omega_0} a_0 - \frac{K}{2a_0^2}\sin\gamma_0\right) a_1 + \left(\frac{K}{2a_0}\cos\gamma_0\right)\gamma_1. \end{aligned} \tag{18}$$

It is worth noting that γ_0 and a_0 satisfy Eq. (14) and we have considered the linear terms in γ_1 and a_1. The right-hand-side (RHS) of Eq. (18) in a matrix form, is used to study the stability of steady-states motions. The resulting characteristic polynomial associated to this matrix can be written in a compact form as follows:

$$\lambda^2 + \mu\lambda + T = 0, \tag{19}$$

where

$$T = \frac{1}{4}\mu^2 + \left[\left(\sigma - \frac{\alpha}{2\omega_0}\right) + \frac{3\alpha}{16\omega_0} a_0^2\right] \cdot \left[\left(\sigma - \frac{\alpha}{2\omega_0}\right) + \frac{\alpha}{16\omega_0} a_0^2\right].$$

Since $\mu > 0$, the steady-state solutions are stable if $T > 0$ and unstable otherwise.

3.2. Superharmonic and subharmonic resonances

Substituting Eq. (6) into Eq. (5) and identifying the coefficients of the same powers, we obtain the following equations to order $O(1)$ and to order $O(\varepsilon)$:

For $O(1)$ order, we have

$$D_0^2 x_0 + \omega_0^2 x_0 = K\omega\sin\left(\omega T_0\right). \tag{20}$$

And for $O(\varepsilon)$ order, we have

$$D_0^2 x_1 + \omega_0^2 x_1 = -2D_0 D_1 x_0 - \mu D_0 x_0 + \frac{1}{6}\alpha x_0^3 - \beta p - \alpha x_0. \tag{21}$$

The resolution of Eq. (20) leads to

$$x_0 = A\left(T_1\right)\exp\left(\mathrm{i}\omega_0 T_0\right) - \mathrm{i}\Lambda\exp\left(\mathrm{i}\omega T_0\right) + \mathrm{CC}, \tag{22}$$

where

$$\Lambda = \frac{1}{2} K\omega\left(\omega_0^2 - \omega^2\right)^{-1}.$$

Replacing the solution x_0 from Eq. (22) into Eq. (21) and taking $\sin\left(\omega\tau\right)$ in the complex form, we obtain the following expression

$$D_0^2 x_1 + \omega_0^2 x_1 = -\left[2\mathrm{i}\omega_0\left(A' + \frac{1}{2}\mu A\right) - \frac{1}{2}\alpha A^2\bar{A} + \alpha A - \alpha A\Lambda^2\right]\exp(\mathrm{i}\omega_0 T_0)$$
$$+\frac{1}{2}\alpha\left\{\frac{1}{3}A^3\exp(3\mathrm{i}\omega_0 T_0)\frac{1}{3}\mathrm{i}\Lambda^3\exp(3\mathrm{i}\omega T_0) - \frac{1}{3}\mathrm{i}A^2\Lambda\exp[\mathrm{i}(2\omega_0+\omega)T_0]\right.$$
$$\left.-\frac{1}{3}\Lambda^2 A\exp[\mathrm{i}(\omega_0-2\omega)T_0] - \mathrm{i}\bar{A}^2\Lambda\exp[\mathrm{i}(\omega-2\omega_0)T_0] - A\Lambda^2\exp[\mathrm{i}(\omega_0+2\omega)T_0]\right\}$$
$$+\Lambda\left[-\mathrm{i}\mu\omega - \mathrm{i}A\bar{A}\alpha - \frac{1}{2}\mathrm{i}\Lambda^2\alpha + \mathrm{i}\alpha\right]\exp(\mathrm{i}\omega T_0) - \beta p + \mathrm{CC}. \tag{23}$$

From Eq. (23), we can obtain two possibles cases of resonance for $\omega = 3\omega_0$ and $3\omega = \omega_0$, which are kindly developed in the following subsection.

3.2.1. Superharmonic resonance

In this case, let us introduce a detuning parameter σ in order to express ω as a function of ω_0, thus let

$$3\omega = \omega_0 + \varepsilon\sigma. \tag{24}$$

There is another term that produces a secular in x_1 in addition to the terms proportional to $\exp(\pm\mathrm{i}\omega_0 T_0)$. We express $3\omega T_0$ in terms of $\omega_0 T_0$ to eliminate the secular terms according to

$$3\omega T_0 = (\omega_0 + \varepsilon\sigma)T_0 = \omega_0 T_0 + \varepsilon\sigma T_0 = \omega_0 T_0 + \sigma T_1, \tag{25}$$

with $T_1 = \varepsilon T_0$. Using Eq. (25) we find that the secular terms in x_1 are eliminated if

$$2\mathrm{i}\omega_0\left(A' + \frac{1}{2}\mu A\right) + \alpha A\left(1-\Lambda^2\right) - \frac{1}{2}\alpha A^2\bar{A} + \mathrm{i}\frac{1}{6}\alpha\Lambda^3\exp(\mathrm{i}\sigma T_1) = 0. \tag{26}$$

Considering Eq. (12) and separating imaginary and real parts, we get

$$\begin{cases} a' = -\dfrac{1}{2}\mu a + \dfrac{\alpha}{6\omega_0}\Lambda^3\cos\gamma, \\ \gamma' a = \dfrac{\alpha}{16\omega_0}a^3 + \left(\sigma - \dfrac{\alpha}{2\omega_0}\left(1-\Lambda^2\right)\right)a - \dfrac{\alpha\Lambda^3}{6\omega_0}\sin\gamma, \end{cases} \tag{27}$$

with $\gamma = \sigma T_1 - \xi$. Setting $a' = \gamma' = 0$ and eliminating γ from Eq. (27) leads to the following response frequency equation

$$\left[\frac{1}{4}\mu^2 + \left(\sigma + \frac{\alpha}{16\omega_0}a^2 - \frac{\alpha}{2\omega_0}\left(1-\Lambda^2\right)\right)^2\right]a^2 = \frac{\alpha^2\Lambda^6}{36\omega_0^2}. \tag{28}$$

In this case the peak amplitude a_p of the free-oscillation term is given by

$$a_\mathrm{p} = \frac{\alpha\Lambda^3}{3\mu\omega_0}. \tag{29}$$

In contrast to the case of primary resonance, a_p is a function of the nonlinear coefficient α, and inversely proportional to μ. However, we also observe that increasing the value of μ consequently induces a decreasing of a_p.

Let us evaluate the stability of the motion of the steady-state from the nature of the singular points of Eq. (27). Substituting Eq. (17) into Eq. (27), developing for the small values of γ_1 and a_1 and considering the linear terms in γ_1 and a_1, we obtain

$$a_1' = -\frac{1}{2}\mu a_1 + \left(\frac{\alpha\Lambda^3}{6}\sin\gamma_0\right)\gamma_1,$$
$$\gamma_1' = \left(-\frac{\alpha}{8\omega_0}a_0 + \frac{\alpha\Lambda^3}{6\omega_0 a_0^2}\sin\gamma_0\right)a_1 - \left(\frac{\alpha\Lambda^3}{6\omega_0 a_0}\cos\gamma_0\right)\gamma_1. \tag{30}$$

The right-hand side (RHS) of Eq. (30) in a matrix form, is used to study the stability of steady-states motion. The resulting characteristic polynomial can be written in a compact form as follows:

$$\lambda^2 + \mu\lambda + T_1 = 0, \tag{31}$$

where

$$T_1 = \frac{1}{4}\mu^2 + \left[\left(\sigma - \frac{\alpha}{2\omega_0}\left(1-\Lambda^2\right)\right) + \frac{3\alpha}{16}a_0^2\right] \times \left[\left(\sigma - \frac{\alpha}{2\omega_0}\left(1-\Lambda^2\right)\right) + \frac{\alpha}{16}a_0^2\right].$$

Since $\mu > 0$, the steady-state solutions are stable if $T_1 > 0$ and unstable otherwise.

3.2.2. Subharmonic resonance

To analyze subharmonic resonances, we follow a similar procedure as previously by introducing a detuning parameter σ to express ω as a function of ω_0

$$\omega = 3\omega_0 + \varepsilon\sigma. \tag{32}$$

The term proportional to $\exp[\pm\mathrm{i}(\omega - 2\omega_0)T_0]$ produces a secular in x_1 in addition to the terms proportional to $\exp(\pm\mathrm{i}\omega_0 T_0)$. Hence, we express $(\omega - 2\omega_0)T_0$ as follows:

$$(\omega-2\omega_0)T_0=(3\omega_0-2\omega_0+\varepsilon\sigma)T_0=\omega_0T_0+\varepsilon\sigma T_0=\omega_0T_0+\sigma T_1 \tag{33}$$

with $T_1=\varepsilon T_0$. Using Eq. (33), we find that the secular terms in x_1 are eliminated if

$$2\mathrm{i}\omega_0\left(A'+\frac{1}{2}\mu A\right)+\alpha A\left(1-\Lambda^2\right)-\frac{1}{2}\alpha A^2\bar{A}+\mathrm{i}\frac{1}{2}\alpha\bar{A}^2\Lambda\exp(\mathrm{i}\sigma T_1)=0. \tag{34}$$

Considering Eq. (12) and separating imaginary and real parts we have

$$\begin{cases} a'=-\dfrac{1}{2}\mu a-\dfrac{\alpha a^2}{8\omega_0}\Lambda\cos\gamma, \\ \gamma' a=\dfrac{3\alpha}{16\omega_0}a^3+\left(\sigma-\dfrac{3\alpha}{2\omega_0}\left(1-\Lambda^2\right)\right)a+\dfrac{3a^2\alpha\Lambda}{8\omega_0}\sin\gamma, \end{cases} \tag{35}$$

where $\gamma=\sigma T_1-3\xi$. Letting $a'=\gamma'=0$ and eliminating γ from Eq. (35) leads to the following frequency–response equation

$$\left[\frac{9}{4}\mu^2+\left(\sigma+\frac{3\alpha}{16\omega_0}a^2-\frac{3\alpha}{2\omega_0}\left(1-\Lambda^2\right)\right)^2\right]a^2=\frac{9\alpha^2a^4\Lambda^2}{64\omega_0^2}. \tag{36}$$

We remark that equation (36) is quadratic in a^2 and its solution is given by: $a^2=p\pm(p^2-q)^{1/2}$, where

$$p=\frac{32\omega_0\sigma}{3\alpha}-12\Lambda^2-16,$$
$$q=\frac{64\omega_0^2}{\alpha^2}\left[\mu^2+\left(\frac{2}{3}\sigma-\frac{\alpha}{\omega_0}(1-\Lambda^2)\right)^2\right].$$

We notice that q is always positive, and thus nontrivial free-oscillation amplitudes occur only for $p\geq 0$ and $p^2\geq q$.

Substituting Eq. (17) into Eq. (35), developing for the small values of γ_1 and a_1 and considering the linear terms in γ_1 and a_1, leads to

$$a_1'=-\frac{1}{2}\mu a_1+\left(\frac{a_0^2\alpha\Lambda}{8}\sin\gamma_0\right)\gamma_1,$$
$$\gamma_1'=\left(\frac{6\alpha}{16\omega_0}a_0-\frac{3\alpha\Lambda}{8\omega_0}\sin\gamma_0\right)a_1+\left(\frac{3\alpha\Lambda a_0}{8\omega_0}\cos\gamma_0\right)\gamma_1. \tag{37}$$

The RHS of Eq. (37) in a matrix form, is used to study the stability of steady-states motion. The resulting characteristic polynomial can be written in a compact form as follows:

$$\lambda^2+2\mu\lambda+T_2=0, \tag{38}$$

where

$$T_2=\frac{3}{4}\mu^2+\left[\left(\frac{\sigma}{3}-\frac{\alpha}{2\omega_0}\left(1-\Lambda^2\right)\right)+\frac{\alpha}{16\omega_0}a_0^2\right]\times\left[\left(\sigma-\frac{3\alpha}{2\omega_0}\left(1-\Lambda^2\right)\right)+\frac{9\alpha}{16}a_0^2\right].$$

Since $\mu>0$, the steady-state solutions are stable if $T_2>0$ and unstable otherwise.

4. Equilibrium points and their stabilities

In this section, we study the stability of the equilibrium points of the system.[27–30] For this reason, let us rewrite the equation of motion (4) as

$$\begin{aligned}\dot{x}_1(\tau)&=x_2(\tau),\\ \dot{x}_2(\tau)&=-\left(\omega_0^2+\alpha\right)x_1(\tau)+\frac{1}{6}\alpha x_1^3(\tau)\\ &\quad-\mu x_2(\tau)-\beta p+K\omega\sin(\omega\tau).\end{aligned} \tag{39}$$

This system can admit AC and DC equilibriums points. By equating the left-hand side of Eq. (39) to zero, an AC equilibrium point $S_{\mathrm{AC}}=(x_0,0)$ is obtained by solving the following equation:

$$x^3+gx+m=0 \tag{40}$$

with $g=[-6\left(\omega_0^2+\alpha\right)]/\alpha$ and $m=(6/\alpha)\left(-\beta p+K\omega\sin(\omega\tau)\right)$. The roots of Eq. (39) can be derived as follows:

$$x_{01}=\frac{-1+\mathrm{i}\sqrt{3}}{2}\times\sqrt[3]{-\frac{g}{2}+\sqrt{\Delta}}+\frac{-1-\mathrm{i}\sqrt{3}}{2}\times\sqrt[3]{-\frac{g}{2}-\sqrt{\Delta}}, \tag{41}$$

$$x_{02}=\sqrt[3]{-\frac{g}{2}+\sqrt{\Delta}}+\sqrt[3]{-\frac{g}{2}-\sqrt{\Delta}}, \tag{42}$$

$$x_{03}=\frac{-1-\mathrm{i}\sqrt{3}}{2}\times\sqrt[3]{-\frac{g}{2}+\sqrt{\Delta}}+\frac{-1+\mathrm{i}\sqrt{3}}{2}\times\sqrt[3]{-\frac{g}{2}-\sqrt{\Delta}}, \tag{43}$$

where

$$\Delta=\left(\frac{g}{2}\right)^2+\left(\frac{m}{3}\right)^3. \tag{44}$$

To solve Eq. (40), we have used the Cardan method whose number of solutions depends on the discriminant delta. As x_0 varies in time, to determine the number of solutions, we will solve numerically the discriminant of Cardan. Figure 4(a) shows us the plot of Cardan's discriminant over time. It was shown in Ref. [31] that:

(i) If $\Delta>0$, equation (40) has one real solution and two complex solutions.

(ii) If $\Delta=0$, the two complex roots in Eqs. (41) and (43) evolve to one real root, leading to the fact that two real roots appear in Eq. (40).

(iii) If $\Delta<0$, equation (40) admits three real solutions, hence the presence of the three equilibrium points.

Figure 4 presents the plot of the Cardan discriminant, the number and the value of the equilibrium points as a function of time.

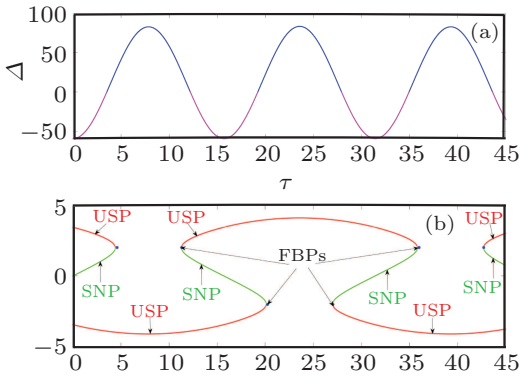


Fig. 4. Cardan discriminant and equilibrium points vary with the evolution of the time for: (a) Cardan discriminant, (b) number and values of equilibrium points. The parameters are $a_1 = 0.21$, $a_2 = 0.001$, $\beta = 20$, $w = 0.2$, $e_0 = 1$, $p = 10^{-3}$, and $a_3 = 0.2$.

On our curve, the blue part represents the values of the positive Cardan discriminant showing the existence of a single equilibrium point given, while the magenta part displays negative values of Cardan discrminant, showing that equation (40) presents three equilibrium points. This result is confirmed by the plot of Fig. 4(b) which allows us to see that in the areas where the Cardan discriminant is negative, the system effectively presents three equilibrium points. On the other hand, in the area where the Cardan discriminant is positive, the system has only one equilibrium point.

These numerical results allow us to confirm the theoretical results with regard to the resolution of a three-degree equation by the Cardan method. In order to study whether the above mentioned equilibrium points are stable or not, we have linearized Eq. (39) around the AC equilibrium point and found that the corresponding Jacobian matrix is defined as

$$J = \begin{bmatrix} 0 & 1 \\ -\alpha - \omega_0^2 + (1/2)\alpha x_0^2 & -\mu \end{bmatrix}, \tag{45}$$

which leads to the following characteristic equation:

$$h(\lambda) = \lambda^2 + \mu\lambda + (\alpha + \omega_0^2) - \frac{1}{2}\alpha x_0^2 = 0. \tag{46}$$

Depending on the eigenvalues at the AC equilibrium point, the stabilities are determined by the sign of the Cardan discriminant Δ. The eigenvalues of the AC equilibrium point are

$$\lambda_{1,2} = -0.5\mu \pm 0.5\sqrt{\mu^2 - 4(\alpha + \omega_0^2) + 2\alpha x_0^2}. \tag{47}$$

Regarding the stability of the equilibrium points, figure 4 shows the stability of all the equilibrium points. Unstable saddle points (USP) in red, stable node points (SNP) in bright green, and fold birfucation point (FBP) in blue. The results obtained are similar to those obtained by Quan Xu *et al.*[32]

Finally, to check the stability of the DC equilibrium point $S_{\mathrm{DC}} = (x_0, 0)$, we set $K\omega\sin(\omega\tau) = 0$, thus we obtained a similar equation as Eq. (40), with $g = -6\left(\omega_0^2 + \alpha\right)/\alpha$ and $m = m' = -(6/\alpha)\beta p$. Following a similar procedure as in the previous case, we obtain

$$x'_{01} = \frac{-1 + \mathrm{i}\sqrt{3}}{2} \times \sqrt[3]{-\frac{g}{2} + \sqrt{\Delta'}} + \frac{-1 - \mathrm{i}\sqrt{3}}{2} \times \sqrt[3]{-\frac{g}{2} - \sqrt{\Delta'}}, \tag{48}$$

$$x'_{02} = \sqrt[3]{-\frac{g}{2} + \sqrt{\Delta'}} + \sqrt[3]{-\frac{g}{2} - \sqrt{\Delta'}}, \tag{49}$$

$$x'_{03} = \frac{-1 - \mathrm{i}\sqrt{3}}{2} \times \sqrt[3]{-\frac{g}{2} + \sqrt{\Delta'}} + \frac{-1 + \mathrm{i}\sqrt{3}}{2} \times \sqrt[3]{-\frac{g}{2} - \sqrt{\Delta'}}, \tag{50}$$

where

$$\Delta' = \left(\frac{g}{2}\right)^2 + \left(\frac{m'}{3}\right)^3. \tag{51}$$

Figure 5 plots the new Cardan discriminant with respect to time using similar parameters as in the previous case. It is observed that the Cardan discriminant is always negative showing that the system always presents three DC equilibrium points.

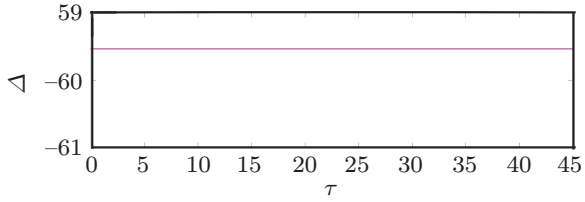


Fig. 5. Evolution of the Cardan discriminant in time. The parameters are $a_1 = 0.21$, $a_2 = 0.001$, $\beta = 20$, $w = 0.2$ $e_0 = 1$, $p = 10^{-3}$, and $a_3 = 0.2$.

5. Effects of parameters on resonant states

In this section, we evaluate the influence of different parameters and the stability in each type of resonance.

5.1. Effects of parameters on primary resonant state

In this subsection, we probe the effect of parameters α, K, μ, σ, and ω_0 on the primary resonant state. Figures 6, 8, 9, 10, 11, 12, and 13 respectively show the influence of the different parameters α, K, μ, σ, and ω_0 on the frequency response curves of the primary resonance in $(\sigma; a)$ space. We note that the amplitude of the response has two branches which curve to the left, most showing the softening behavior. The lower branch presents unstable and stable solutions while the upper branch presents stable solutions. From these figures, we note the presence of jump, hysteresis, and resonance phenomena with the increase in external excitation. These are the important characteristics showing the existence of nonlinear phenomena in the circuit.

We present in Fig. 6 the comparison between the existence ($\alpha > 0$) and the absence ($\alpha = 0$) of the nonlinear parameter α. This comparison is obtained by solving numerically or analytically Eq. (15). These curves show us that the amplitude reaches its maximum when the detuning parameter becomes zero. The peak amplitude given by the equation Eq. (16) is independent of the value of the nonlinear parameter α. The nonlinear results are symmetrical to this order of approximation and represent the solution in a very narrow band around the resonant frequency, so that the scale σ is considerably extended. We observed that in the presence of a nonlinearity, the dynamics of the junction turn to the left, presenting here magenta the hysteresis and jump phenomena and in the absence of nonlinearity, the dynamics of our MJJ present only the resonance phenomenon. The nonlinearity effects seem to bend the curve amplitude.

Similarly, in these figures, we present the analytical (red curve) and numerical (blue curve) results. We notice a perfect similarity between these two results, which allows us to confirm our analytical resolution method.

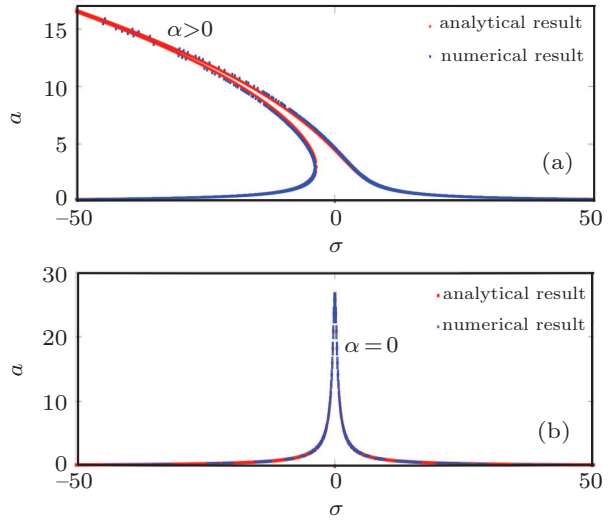


Fig. 6. Comparison of linear and nonlinear response curves, analytical, and numerical results: amplitude response. In panels (a) and (b): $\mu = 0.75$, $\beta = 0.5$, $\omega_0 = 1$, $\varepsilon = 10^{-6}$, $p = 0.1$, and $K = 10$.

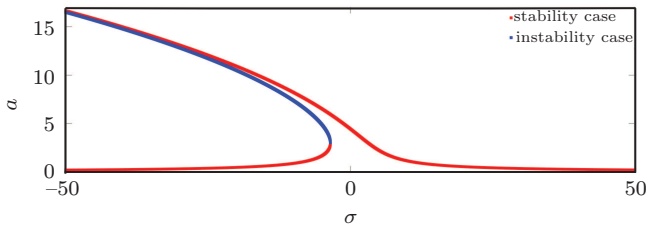


Fig. 7. Stability curves of the harmonic oscillations of the system for the nonlinearity parameter $\alpha > 0$. The red curve stands for the stable solution and the blue curve represents the unstable solution. $\omega_0 = 1$, $\alpha = 3$, $\mu = 0.75$, and $K = 20$.

Figure 7 presents the solutions of stability (curve in red) and instability (curve in blue) of the dynamics of the junction. This curve has been plotted only for positive value of α. By observing this figure, we note that for the values of the detuning parameter, the solutions of stability and instability are separated in a certain zone.

In addition, figure 8 shows that the nonlinearity bends the frequency–response curve away from the linear curve ($\alpha = 0$), to the right for hard spring (*i.e.*, $\alpha < 0$) and to the left for soft spring (*i.e.*, $\alpha > 0$). Moreover the maximun amplitude of the response stays unchanged but its location value increases. We also noticed that for ($\alpha = 0$), we have the resonance phenomenon, and for ($\alpha \neq 0$) we have the jump and hysteresis phenomena.

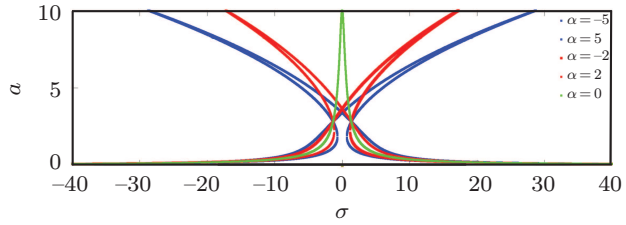


Fig. 8. Frequency response curves for primary resonance of MJJ equation: effect of the nonlinearity parameter. In this figure, we take $\omega_0 = 1$, $K = 10$, $\alpha = 3$, and $\mu = 0.75$.

Figure 9 shows the variation of the frequency–response curve with the amplitude of the external excitation for the soft spring. We note that when the value of K increases, the maximum amplitude response increases highly as well as the instability region. As the amplitude of the external excitation increases, the frequency–response curves band away from the zero axis. We observed that, depending on the value of K, some of the frequency–response curves are of single valued while others are multivalued. We also note that, the increase in the excitation parameter K allows us to have the hysteresis and amplitude jump phenomena.

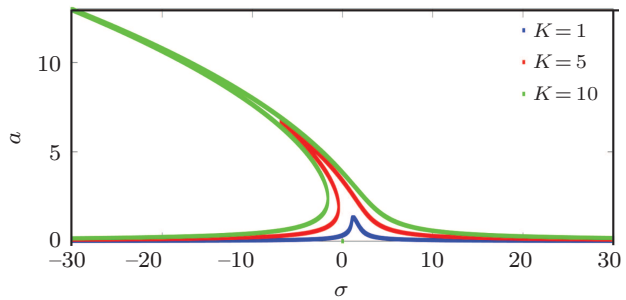


Fig. 9. Frequency–response curves for primary resonances of MJJ equation: the effect of the amplitude of the external excitation by taking $\omega_0 = 1$, K=10, $\alpha = 3$, and $\mu = 0.75$.

Figure 10 shows the effect of the damping parameter μ. We note that when μ increases, the maximun amplitude response decreases. This curve presents the softening behavior. We also noticed the appearance of the jump and hysteresis phenomena.

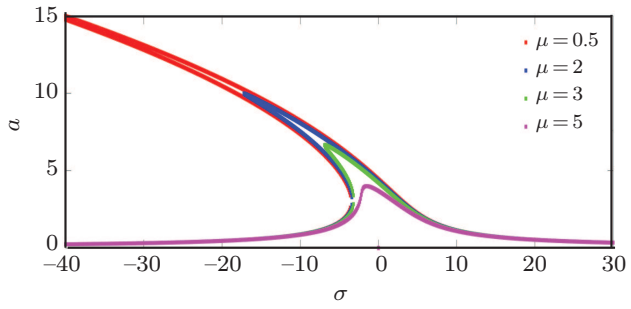


Fig. 10. The effect of the damping on the frequency response of the modified Josephson junction equation to a primary-resonance by taking $\omega = 1$, $K = 5$, and $\alpha = 2$.

Figure 11 shows the variation of the amplitude response with the amplitude of the excitation for several values of σ. The values of α and μ are the same for all curves. These curves are obtained from Eq. (15). We note that depending on the value of σ, some curves are multivalued while others are single-valued. The amplitude-response is a linear function of K and the slope decreases when σ increases. The hysteresis phenomenon appears for the value of σ and disappears when σ increases.

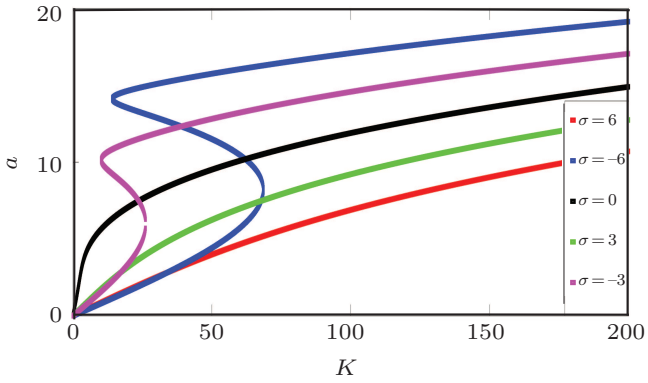


Fig. 11. The effect of detuning parameter on the amplitude– response curve and frequency–response curve for primary resonances of MJJ equation: the effect of detuning parameter, $\omega = 1$, $\alpha = 0.5$, $\mu = 1$.

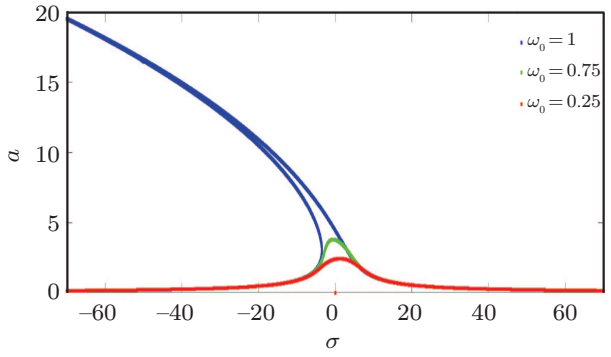


Fig. 12. The effect of the proper frequency on the amplitude response curves with $K = 20$, $\alpha = 1$, and $\mu = 1$.

Figure 12 presents the plot of the amplitude response as a function of the detuning parameter for several values of the proper frequency and for a fixed value of the excitation force amplitude K. We observed that the decrease in the ω_0 frequency decreases the peak amplitude. We also note the presence of hysteresis and amplitude jump phenomena with the increase in the value ω_0.

Figure 13 displays the plot of the amplitude response as a function of the detuning parameter for several values of the excitation force amplitude K, and for a fixed value of the proper frequency. It is observed that an increasing in the value of K increases the peak amplitude. We also note the presence of hysteresis and amplitude jump phenomena with the increase of the value of K .

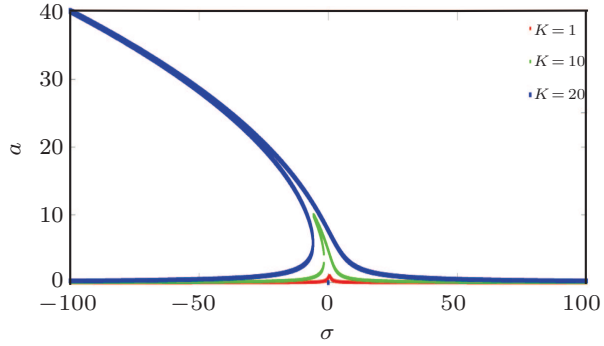


Fig. 13. The effect of the external excitation on the amplitude response curves with $\omega_0 = 1$, $\alpha = 1$, and $\mu = 1$.

5.2. Effects of parameters on superharmonic resonance

In Figs. 14, 15, 16, 17, and 18, various frequency–response curves are shown. These curves show the influence of the parameters α, Λ, and μ. Here as in the case of primary resonance, the bending of the frequency–response curves is responsible of the jump phenomenon.

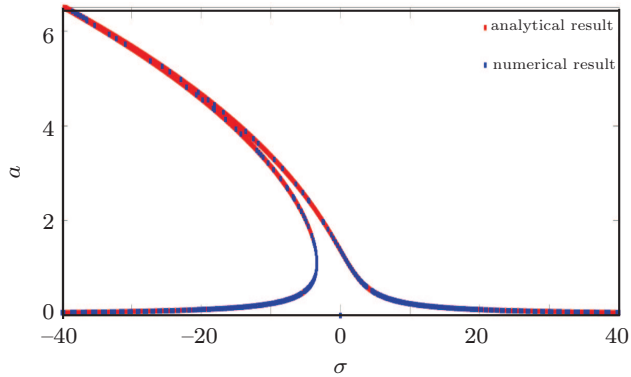


Fig. 14. Frequency–response curves for superharmonic resonance of MJJ equation: analytical and numerical results for $\omega_0 = 5$, $\Lambda = 1$, K=70, $\varepsilon = 10^{-6}$, $\mu = 0.75$, $\alpha = 3.00$, $\beta = 0.5$, and $p = 0.1$.

In Fig. 14, the frequency–response curve is plotted for a positive nonlinear parameter ($\alpha > 0$). This curve is obtained by analytically or numerically solving Eq. (28). The maximum amplitude given by Eq. (29) is independent of the value of the nonlinearity parameter α. We observed that, due to the nonlinear term, the dynamics of the JJ turn to the left, depicting the

hysteresis and jump phenomena. It turns out that in the neighborhood of the resonant frequency, the system can accumulate energy.

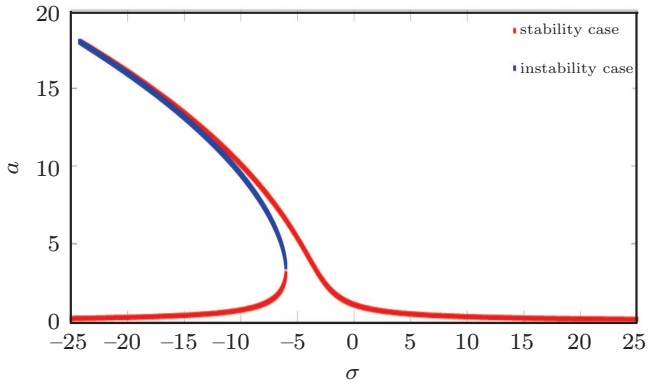


Fig. 15. Stability curves of the harmonic oscillations of the system for the nonlinearity parameter $\alpha > 0$. The red curve stands for the stable solution and the blue curve represents the unstable solution. The other parameters are: $\omega_0 = 3$, $\Lambda = 3$, $\mu = 0.5$, and $\alpha = 3$.

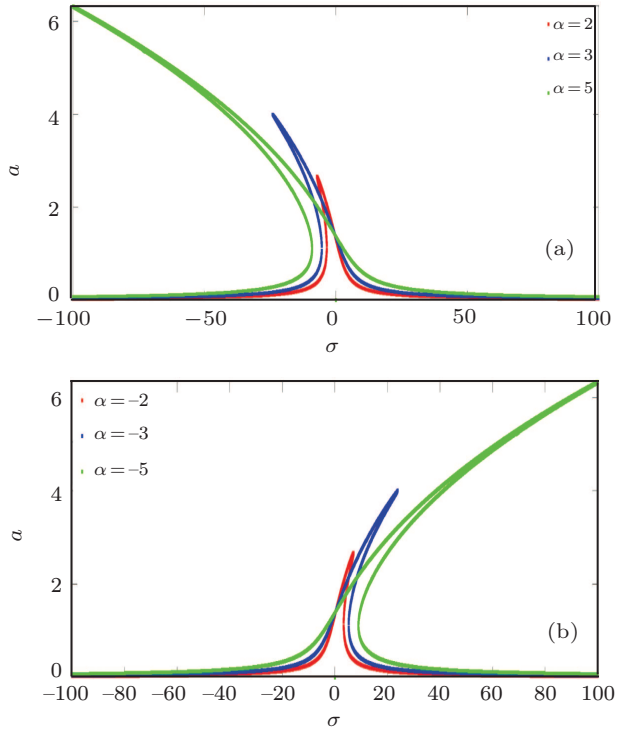


Fig. 16. Frequency–response curves for superharmonic resonance of MJJ equation: the effect of the nonlinearity parameter for $\omega_0 = 3$, $\Lambda = 1$, and $\mu = 2$.

As in the case of primary resonance, these figures present the analytical (red curve) and numerical (blue curve) results. We note a perfect similarity between these two results, which allows us to confirm our analytical resolution method.

Figure 15 presents the solutions of stability (curve in red) and instability (curve in blue) of the dynamics of the junction. This curve has been plotted only for positive α. Observing this figure, we can conclude that for different values of the detuning parameter, the solutions of stability and instability are separated in a certain zone displaying the dynamic of the junction.

In Fig. 16, we noted that the system exhibits hardening behavior when α becomes negative. The upper and lower branches have stables solutions. When α increases, the maximum amplitude decreases highly and the corresponding curves move to the right with respect to typical frequency response curves with negative values of α. For positive values of α, softening behavior is obtained and the maximum amplitude of the response decreases with decreasing of α.

Figure 17 shows the effect of the excitation amplitude Λ. We realize that when Λ decreases, maximum amplitude of the response decreases. The system displays softening behavior and therefore it appears in such systems the jump and hysteresis phenomena.

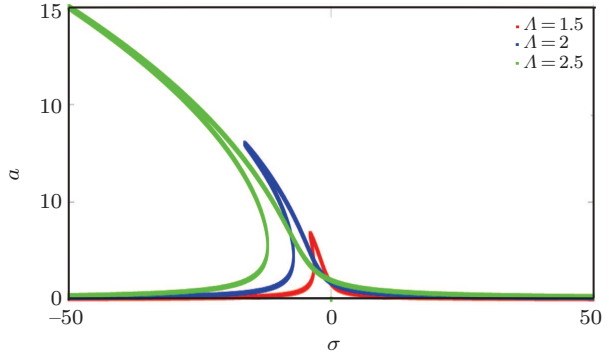


Fig. 17. The effect of amplitude of excitation Λ on the frequency–response curve of the superharmonic resonance for $\omega_0 = 1$, $\mu = 1$, and $\alpha = 3$.

Figure 18 presents the effect of the nonlinear damping coefficient. We observed that, when the nonlinear damping coefficient increases, the maximum amplitude responses decreases considerably, and the hysteresis phenomenon becomes more pronounced.

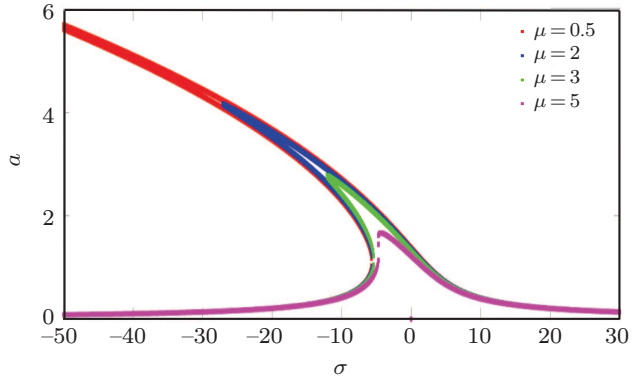


Fig. 18. The effect of the damping on the frequency response of the MJJ equation to a superharmonic resonance for $\omega_0 = 3$, $\Lambda = 1$, and $\alpha = 5$.

5.3. Effects of parameters on subharmonic resonance

In this subsection, we search for the effects of the parameters μ, σ, K, and α on subharmonic resonance. Figsures 19, 20, 21, 22, 23, 24 show the frequency–response curve for the

variations of the parameters μ, σ, K, and α in the subharmonic resonance. All these curves present an hysteresis phenomenon, and in contrast to the primary and superharmonic resonances, there is not amplitude jump.

Figure 19 shows the effect of the positive nonlinearity parameter (*i.e.*, $\alpha > 0$). It is obtained analytically by solving Eq. (36). We observed that this parameter turns the curve to the left showing softening behavior. This curve presents the results obtained analytically (curve in red) and numerically (curve in blue). We also notice a coincidence between both results, which confirms our numerical simulation and analytical resolution method.

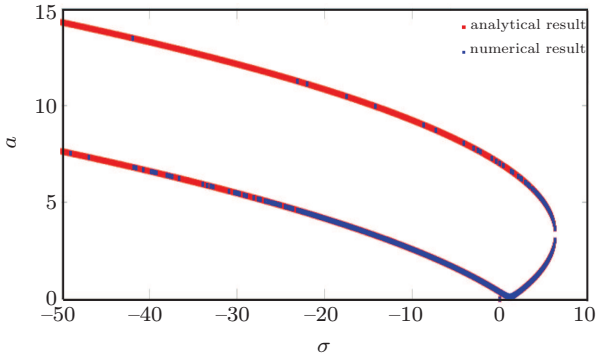


Fig. 19. The frequency–response curves for subharmonic resonance of the MJJ equation: analytical and numerical results for $\omega_0 = 5$, $\omega = 2$, $p = 0.1$, $\beta = 0.8$, $\varepsilon = 10^{-6}$, $\mu = 0.25$, and $\alpha = 3$.

Figure 20 is plotted by analytically solving the nonlinear algebraic Eq. (36) taking into consideration of the condition of stability Eq. (38). This figure presents the plot of the stability condition of the MJJ in the subharmonic case. We observed on this plot two branches oriented to the left: one for unstable (curve in blue) and the other for stable (curve in red).

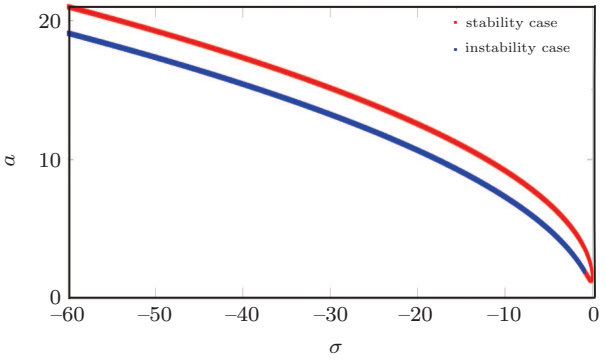


Fig. 20. Stability curves of the harmonic oscillations of the system for the nonlinearity parameter $\alpha > 0$. The red curve stands for the stable solution and the blue curve represents the unstable solution. $\omega_0 = 5$, $\omega = 2$, $K = 40$, and $\mu = 0.25$.

Figure 21 shows the effect of damping parameter for subharmonic resonance. We observed that the amplitude response has a multivalued continuous curve represented by semi-oval. For further increasing of μ respectively (*i.e.*, μ takes the values 0.5, 2, 3, and 5), we note that the semi-oval is contracting respectively. In addition, the lower and the upper branches magnitudes of the semi-oval are respectively increased and decreased.

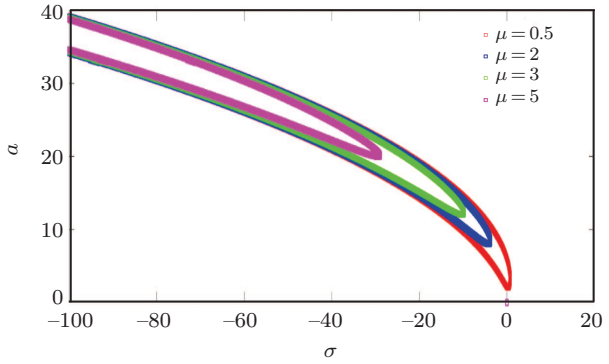


Fig. 21. Subharmonic response for the MJJ equation, amplitude oscillation term *versus* detuning: the effect of damping for $\omega_0 = 5$, $\omega = 0.1$, $K = 5$, and $\alpha = 2$.

Figure 22 shows the effect of detuning parameter for subharmonic resonance. Similar phenomenon is observed in Fig. 21 concerning the response amplitude. For further increasing of σ respectively (*i.e.*, σ taking the values 0.1, 0.5, and 1), we note that the semi-oval is contracted respectively. The lower and the upper branches magnitudes of the semi-oval are respectively increased and decreased too.

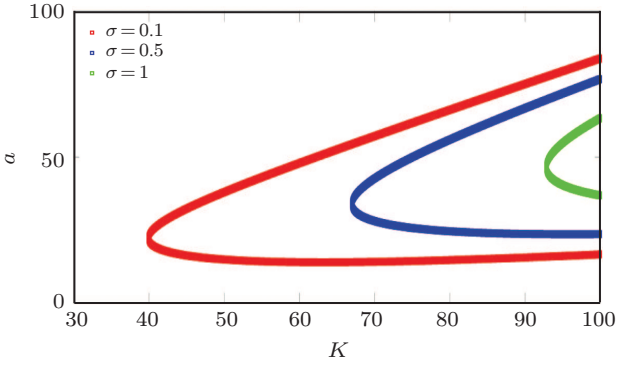


Fig. 22. Subharmonic response for the MJJ equation, amplitude oscillation term *versus* amplitude of the excitation: the effect of detuning for $\omega_0 = 2$, $\omega = 0.01$, $\mu = 0.25$, and $\alpha = 0.01$.

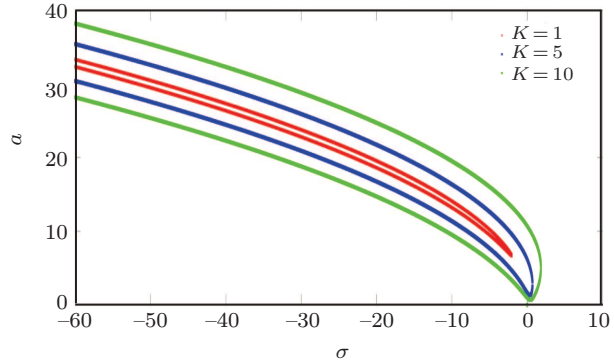


Fig. 23. Subharmonic response for the MJJ equation, amplitude oscillation term *versus* detuning: the effect of amplitude of excitation for $\omega_0 = 5$, $\omega = 0.1$, $\mu = 0.25$, and $\alpha = 1.5$.

Figure 23 shows the effect of amplitude response of excitation for subharmonic resonance. We observed that the amplitude response has multivalued continuous curve represented

by semi-oval. For further decreasing of K respectively (*i.e.*, K taking the values 10, 5, and 1), we notice similar phenomenon as in Fig. 22 regarding the lower and upper semi-oval branches magnitudes.

Figure 24 presents the plot of the amplitude response as a function of the detuning parameter σ obtained for different values of the parameter α ($\alpha > 0$ and $\alpha < 0$) nonlinearity parameter. We note that each curve has two lower and upper branches. For positive values of α, the curves are bent to the left showing softening behavior, on the other hand for negative values of α, the curves are oriented to the right presenting hardening behavior.

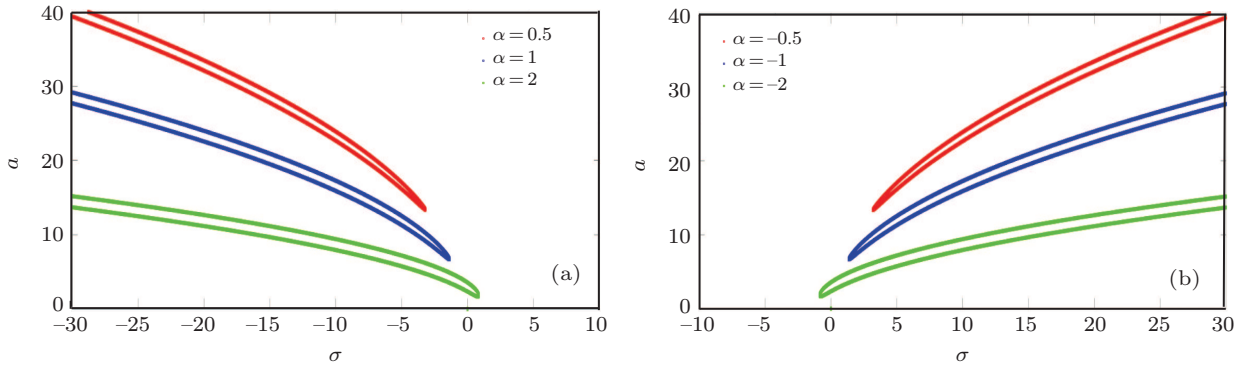


Fig. 24. Subharmonic response for the MJJ equation, amplitude oscillation term *versus* detuning: the effect of nonlinearity parameter for $\omega_0 = 5$, $\omega = 2$, $K = 10$, and $\mu = 0.25$.

6. Conclusion

This paper presents a modified Josephson junction (MJJ) model and its equivalent electrical diagram, which presents a nonlinear differential equation with a proper frequency. The analysis of nonlinear resonances of the MJJ was studied using the multiple time scale method. It followed that the Josephson junction (JJ) with a proper frequency has three states of resonance namely, the primary resonance, the superharmonic resonance and the subharmonic resonance. The effects of the system's parameters on each type of resonance were quietly studied analytically. Numerical results obtained showed that the system exhibits hardening and softening behaviors. In addition, we also noticed the appearance of hysteresis phenomena and jump amplitude. Stable and unstable solutions in each type of resonance have been highlighted, thus showing the possibility of controlling the dynamics of the JJ. The stability of equilibrium points were kindly investigated. Furthermore, it has been shown that system's parameters can be used to control the magnitude of the system's nonlinear response.

References

[1] Siewe M S, Tchawoua C and Rajasekar S 2012 *Commun. Nonlinear Sci. Numer. Simul.* **17** 4485

[2] Miwadinou C H, Monwanou A V and Orou J B C 2015 *Int. J. Bifur. Chaos* **25** 1550024

[3] Strogatz S 2001 *Nonlinear Dynamics And Chaos: With Applications To Physics, Biology, Chemistry, And Engineering (Studies in Nonlinearity)* (Westview Press)

[4] Monwanou A V, Miwadinou C H, Hinvi L and Orou J B C 2017 *Int. J. Sci. Eng. Appl. Sci.* **88** 97 ISBN: 2395-3470

[5] Pandey M, Rand R H and Zehnder A T 2007 *International Design Engineering Technical Conferences* paper No. DETC2007-34411, pp. 893–903

[6] Bi Q 2004 *Int. J. NonLinear Mech.* **39** 33

[7] Li S, Niu J and Li X 2018 *Chin. Phys. B* **27** 120502

[8] Mitsi S, Natsiavas S and Tsiafis I 1998 *Nonlinear Dyn.* **16** 23

[9] Natsiavas S 1994 *Nonlinear Dyn.* **6** 69

[10] Nayfeh A H 2011 *Introduction to perturbation techniques* (John Wiley and Sons)

[11] Mishra A, Saha S, Hens C, Roy P K, Bose M, Louodop H, Cerdeira H A and Dana S K 2017 *Phys. Rev. E* **95** 010201

[12] Domínguez D and Cerdeira H A 1995 *Phys. Rev. B* **52** 513

[13] Domínguez D and Cerdeira H A 1995 *Phys. Lett. A* **200** 43

[14] Domínguez and Cerdeira H A 1993 *Phys. Rev. Lett.* **71** 3359

[15] Tang J S, Fu W B and Li K A 2002 *Chin. Phys.* **11** 1004

[16] Levi M, Hoppensteadt F C and Miranker W L 1978 *Q. Appl Math.* **36** 167

[17] Josephson B 1962 *Phys. Lett.* **1** 251

[18] Zharkov G and Altudov Y K 1978 *Sov. Phys. JETP* **47** 901

[19] Tsang K Y and Schwartz I B 1992 *Phys. Rev. Lett.* **68** 2265

[20] Duwel A E, Watanabe S, Triá E, Orlando T P, van der Zant H S J and Strogatz S H 1997 *J. Appl. Phys.* **82** 4661

[21] Duwel A E, Triá E, Orlando T P, van der Zant H S J, Watanabe S and Strogatz S H 1996 *J. Appl. Phys.* **79** 7864

[22] Goldobin E, Koelle D, Kleiner R and Buzdin A 2007 *Phys. Rev. B* **76** 224523

[23] Krantz P, Reshitnyk Y, Wustmann W, Bylander J, Gustavsson S, Oliver W D, Duty T, Shumeiko V and Delsing P 2013 *New J. Phys.* **15** 105002

[24] Louodop P, Tchitnga R, Fagundes F F, Kountchou M, Tamba V K, Carlos L P L and Cerdeira H A 2019 *Phys. Rev. E* **99** 105002

[25] You J Q and Nori F 2011 *Nature* **474** 589

[26] Kaplunenko V and Fischer G M 2004 *Supercond. Sci. Technol.* **17** S145

[27] Chen M, Xu Q, Lin Y and Bao B 2016 *Nonlinear Dyn.* **87** 789

[28] Xu Q, Zhang Q, Qian H, Wu H and Bao B 2018 *Int. J. Cir. Theor. Appl.* **46** 1917

[29] Bao B, Luo J, Bao H, Chen C, Wu H and Xu Q 2019 *Int. J. Bifur. Chaos* **29** 1950168

[30] Luo J, Bao H, Chen M, Xu Q and Bao B 2019 *Eur. Phys. J. S. T.* **228** 1983

[31] Han X, Chen Z and Bi Q 2016 *Chaos* **26** 023117

[32] Xu Q, Zhang Q, Bao B and Hu Y 2017 *IEEE* **5** 21039